

Semiparametric Functional Factor Models with Bayesian Rank Selection

Daniel R. Kowal*

Abstract

Functional data are frequently accompanied by parametric templates that describe the typical shapes of the functions. Although the templates incorporate critical domain knowledge, parametric functional data models can incur significant bias, which undermines the usefulness and interpretability of these models. To correct for model misspecification, we augment the parametric templates with an infinite-dimensional nonparametric functional basis. Crucially, the nonparametric factors are regularized with an ordered spike-and-slab prior, which implicitly provides rank selection and satisfies several appealing theoretical properties. This prior is accompanied by a parameter-expansion scheme customized to boost MCMC efficiency, and is broadly applicable for Bayesian factor models. The nonparametric basis functions are learned from the data, yet constrained to be orthogonal to the parametric template in order to preserve distinctness between the parametric and nonparametric terms. The versatility of the proposed approach is illustrated through applications to synthetic data, human motor control data, and dynamic yield curve data. Relative to parametric alternatives, the proposed semiparametric functional factor model eliminates bias, reduces excessive posterior and predictive uncertainty, and provides reliable inference on the effective number of nonparametric terms—all with minimal additional computational costs.

KEYWORDS: factor analysis; nonparametric regression; shrinkage prior; spike-and-slab prior; yield curve

*Dobelman Family Assistant Professor, Department of Statistics, Rice University (daniel.kowal@rice.edu).

1 Introduction

1.1 Setting and goals

As high resolution monitoring and measurement systems generate vast quantities of complex and highly correlated data, *functional data analysis* has become increasingly vital for many scientific, medical, business, and industrial applications (Ullah and Finch, 2013). Functional data are (noisy) realizations of random functions $Y_i, i = 1, \dots, n$ observed over a continuous domain, such as time, space, or wavelength, and exhibit a broad variety of shapes. The concurrence of *complex* and *voluminous* data prompts the common use of nonparametric models for functional data (Ramsay and Silverman, 2005). Yet in many applications, there is valuable information regarding the functional form of Y_i . Template curves that describe the shape of Y_i are derived from fundamental scientific laws or motivated by extensive empirical studies, and often are the focal point of the analysis. Prominent examples include human motor control (Ramsay, 2000; Ramsay et al., 1995; Goldsmith and Kitago, 2016), yield curves and interest rates (Nelson and Siegel, 1987; Diebold and Li, 2006; Cruz-Marcelo et al., 2011), and basal body temperature (Scarpa and Dunson, 2009, 2014; Canale et al., 2017).

Our goal is to construct a functional data modeling framework that simultaneously (i) incorporates parametric templates in a coherent and interpretable manner, (ii) maintains the modeling flexibility of nonparametric methods, and (iii) provides computationally scalable inference with reliable uncertainty quantification. The approach is fully Bayesian, accompanied by an efficient MCMC algorithm for posterior and predictive inference, and equally applicable to both densely-observed and sparsely- or irregularly-sampled functional data.

The parametric templates are represented as a spanning set $\mathcal{H}_0 = \text{span}\{g_1(\cdot; \gamma), \dots, g_L(\cdot; \gamma)\}$ of functions $\{g_\ell(\cdot, \gamma)\}_{\ell=1}^L$ known up to γ . Any function belonging to \mathcal{H}_0 is a linear combination of $\{g_\ell\}$; the corresponding coefficients and the parameters γ must be learned. Important examples are presented in Table 1. The linear basis is routinely used for longitudinal data

analysis and here is equivalent to a random slope model (Molenberghs and Verbeke, 2000). A change in slope, $(\tau - \gamma)_+$ with $(x)_+ = \max\{0, x\}$, is useful for modeling structural changes, such as a change in disease transmissions due to policy interventions (Wagner et al., 2020). Cosinor functions model circadian rhythms (Mikulich et al., 2003) and other periodic behaviors (Welham et al., 2006). Biphasic curves offer utility in modeling basal body temperature of women during the menstrual cycle (Scarpa and Dunson, 2009, 2014; Canale et al., 2017). In general, interest centers on learning the linear coefficients associated with each g_ℓ , the nonlinear parameters γ , and an adequate yet interpretable model for the functions Y_i .

Linear	Linear change	Cosinor	Biphasic
$\{1, \tau\}$	$\{1, \tau, (\tau - \gamma)_+\}$	$\{1, \sin(2\pi\tau/\gamma), \cos(2\pi\tau/\gamma)\}$	$\{1, \exp(\gamma\tau)/\{1 + \exp(\gamma\tau)\}\}$

Table 1: Examples of parametric templates, or spanning sets, for \mathcal{H}_0 .

The advantages of the parametric templates are clear: they incorporate domain knowledge, lend interpretability to the model, and often produce low-variance estimators relative to nonparametric alternatives. These templates are restrictive by design, and therefore can incur significant bias and other model misspecifications. Such effects erode model interpretability and can induce variance inflation. For illustration, we present model fits for two datasets in Figure 1 using a parametric model and our proposed semiparametric alternative; details and analyses of these data are in Section 6. In both instances, the templates capture the general shape of the data. However, regions of substantial bias are present, which produce uniformly inflated prediction bands over the domain. By comparison, the proposed approach preserves the essential shape of the curves, yet corrects the bias and shrinks the prediction bands appropriately—and crucially does so without overfitting.

1.2 Overview of the proposed approach

The *semiparametric functional factor model* (SFFM) bridges the gap between parametric and nonparametric functional data models. The SFFM augments a parametric template \mathcal{H}_0

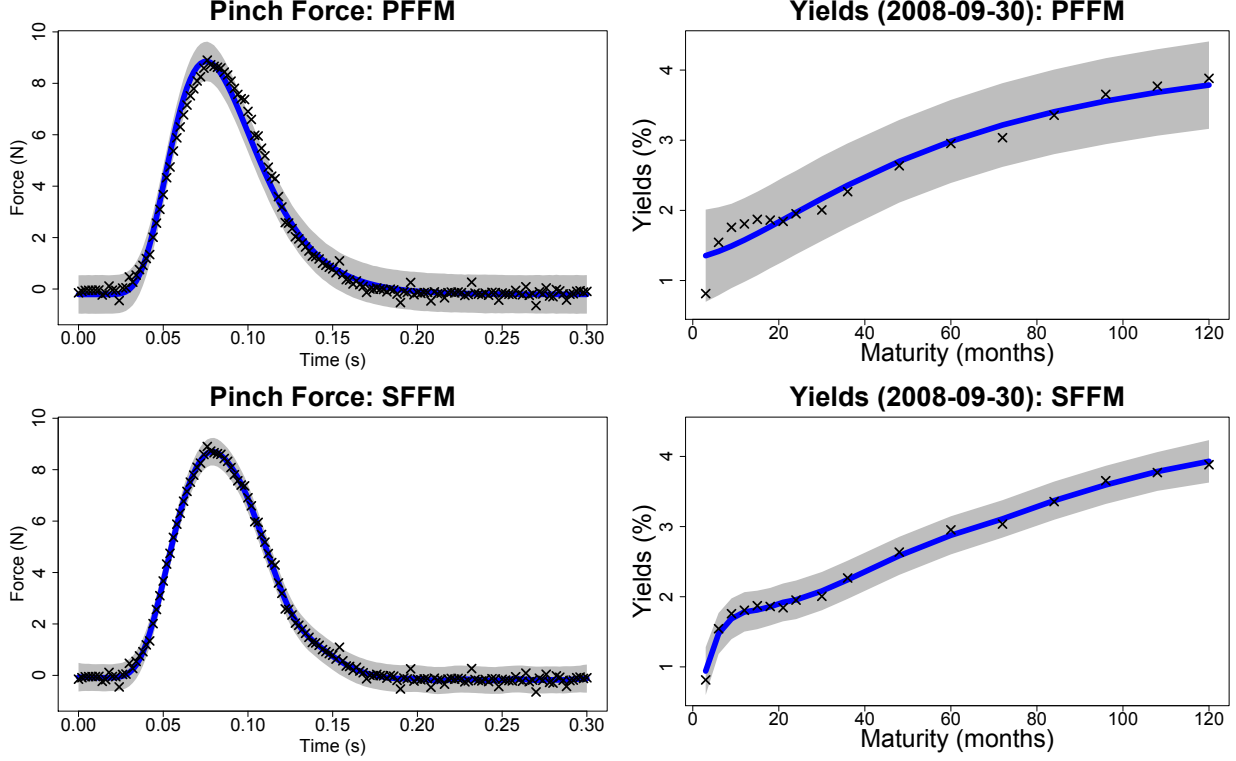


Figure 1: Posterior expectations and 95% simultaneous prediction bands for the parametric (PFFM, top) and semiparametric functional factor model (SFFM, bottom) for one replicate of the pinch force data (left; see Section 6.1) and one yield curve (right; see Section 6.2). The proposed SFFM corrects the bias of the PFFM and offers narrower prediction bands.

with a nonparametric and infinite-dimensional basis expansion for the functions $Y_i \in L^2(\mathcal{T})$:

$$Y_i(\tau) = \sum_{\ell=1}^L \alpha_{\ell,i} g_{\ell}(\tau; \gamma) + \sum_{k=1}^{\infty} \beta_{k,i} f_k(\tau), \quad \tau \in \mathcal{T}, \quad (1)$$

where $\{f_k\}$ are unknown nonparametric functions, $\{\alpha_{\ell,i}\}$ and $\{\beta_{k,i}\}$ are unknown factors for the parametric and nonparametric components, respectively, and $\mathcal{T} \subset \mathbb{R}^d$ is the domain, usually with $d = 1$ for curves or $d = 2$ for images. Without the nonparametric terms, (1) is a *parametric functional factor model* (PFFM), which serves as our parametric baseline.

Our implementation of (1) is fully Bayesian with three unique and essential features.

First, the nonparametric basis $\{f_k\}$ is treated as unknown. The SFFM pools information

across all functions $\{Y_i\}$ to learn the key functional features in the data—in particular, the systemic biases unresolved by \mathcal{H}_0 . The functions $\{f_k\}$ are learned jointly with the parametric terms γ and $\{\alpha_{\ell,i}\}$ and the nonparametric factors $\{\beta_{k,i}\}$. A variety of models for each f_k are compatible within this framework, such as splines, wavelets, or Gaussian processes, while uncertainty about $\{f_k\}$ is automatically absorbed into the joint posterior distribution.

Second, the nonparametric factors $\{\beta_{k,i}\}$ are endowed with an ordered spike-and-slab prior distribution. The proposed prior is critical for coherence of the infinite-dimensional basis expansion in (1): it provides much-needed regularization, encourages selection of a finite number of factors, and provides posterior inference for the effective number of nonparametric terms—including an assessment of whether any nonparametric component is needed at all. The prior admits a parameter expansion that offers substantial improvements in MCMC efficiency and satisfies several key properties that broaden applicability beyond the SFFM.

Third, the nonparametric basis $\{f_k\}$ is constrained to be orthogonal to the templates $\{g_\ell\}$. This important constraint enforces distinctness between the parametric and nonparametric components of the SFFM, which preserves the interpretability of the parametric model. The nonredundancy of $\{f_k\}$ is also essential for valid inference on the effective number of nonparametric terms. As an added benefit, the orthogonality constraint produces computational simplifications that improve both the algorithmic efficiency and the ease of implementation of the MCMC algorithm.

The SFFM in (1) is accompanied by an observation error equation to accommodate noisy and sparsely- or irregularly-sampled functional data. The observed data $\mathbf{y}_i = (y_{i,1}, \dots, y_{i,m_i})'$ are modeled as noisy realizations of Y_i on a discrete set of points $\{\tau_{i,j}\}_{j=1}^{m_i} \subset \mathcal{T}$ for $i = 1, \dots, n$:

$$y_{i,j} = Y_i(\tau_{i,j}) + \epsilon_{i,j}, \quad \epsilon_{i,j} \overset{\text{indep}}{\sim} N(0, \sigma_\epsilon^2), \quad (2)$$

although non-Gaussian versions are available (Goldsmith et al., 2015; Kowal, 2019). We

proceed using common observation points $\tau_{i,j} = \tau_j$ and $m_i = m$ for notational simplicity, but this restriction may be relaxed.

Although we focus on the parametric and semiparametric versions of (1), the proposed modeling framework remains useful without any parametric template ($L = 0$). In this case, (1) resembles a Karhunen-Loève decomposition, and $\{f_k\}$ correspond to the eigenfunctions of the covariance function of $\{Y_i\}$ (assuming the functions Y_i have been centered). The Karhunen-Loève decomposition provides the theoretical foundation for functional principal components analysis (FPCA), which is widely used in functional data analysis. As such, model (1)—together with the model for $\{f_k\}$ and the ordered spike-and-slab prior for $\{\beta_{k,i}\}$ —constitutes a new approach for Bayesian FPCA (Suarez and Ghosal, 2017) or functional factor modeling (Montagna et al., 2012; Hays et al., 2012; Kowal et al., 2017a).

1.3 Review of related approaches

Semiparametric models for functional data have appeared primarily in the frequentist literature. For modeling a single function, L-splines incorporate a favored space of parametric functions \mathcal{H}_0 by combining a goodness-of-fit criterion with a penalty on deviations from \mathcal{H}_0 (Ramsay and Dalzell, 1991; Heckman and Ramsay, 2000). The elegance of L-splines emanates from reproducing kernel Hilbert space (RKHS) theory: by specifying a RKHS and a penalty operator with null space \mathcal{H}_0 , the Riesz representation theorem induces an expansion of the form (1), where only m basis functions $\{f_k\}_{k=1}^m$ are needed and can be derived analytically (Wang, 2011). However, these derivations are highly challenging for all but the simplest choices of \mathcal{H}_0 , which inhibits widespread practical use. In addition, L-splines offer limited direct inference on the adequacy of the parametric templates \mathcal{H}_0 , and typically require hypothesis tests with asymptotic validity. By comparison, the proposed SFFM learns $\{f_k\}_{k=1}^\infty$ directly from the data—which sidesteps the challenging derivations—and provides direct posterior inference on the effective number of nonparametric terms.

Other non-Bayesian approaches for semiparametric functional data analysis seek to replace nonparametric functions with parametric alternatives. Sang et al. (2017) attempt to simplify FPCA by using polynomials for each FPC instead of splines or Fourier functions. In functional regression analysis, Chen et al. (2019) develop hypothesis tests to determine whether an unknown regression function deviates from a parametric template.

Bayesian semiparametric functional data models are less common. The “semiparametric” model of Lee et al. (2018) refers to additive rather than linear effects, but does not include a parametric template like \mathcal{H}_0 . Scarpa and Dunson (2009) construct a Dirichlet process mixture of a parametric function and a Gaussian process contamination, which is generalized by Scarpa and Dunson (2014) to include prior information on the frequencies of certain functional features. These methods are designed primarily for clustering: they identify individual curves Y_i that deviate substantially from the parametric model, while the remaining curves are presumably well modeled parametrically. The SFFM is capable of modeling total deviations from \mathcal{H}_0 for a particular Y_i , but also captures—and corrects—partial deviations from \mathcal{H}_0 that persist for some or many Y_i . Unlike the mixture models, the SFFM is well suited for including additional layers of dependence, such as hierarchical (Section 6.1) or dynamic (Section 6.2) models, while maintaining efficient posterior computing.

Functional factor models such as (1) require rank selection. In FPCA, the rank is usually selected to explain a pre-specified proportion of variability in the data. This approach is not compatible with fully Bayesian inference and is complicated by the presence of the parametric templates in (1), which include unknown parameters. Information criteria such as WAIC (Watanabe, 2010) offer metrics for model comparisons, but require separate model fits for each rank. Multiplicative gamma process priors (Bhattacharya and Dunson, 2011) can reduce sensitivity to the choice of the rank (Montagna et al., 2012; Kowal and Bourgeois, 2020), but are known to induce undesirable overshrinkage in certain settings (Durante, 2017) and do not provide direct estimation or uncertainty quantification for the rank. The proposed

ordered spike-and-slab prior resolves these issues and provides computationally efficient and interpretable posterior inference on the rank on the nonparametric term in (1).

The remainder of the paper is organized as follows. We introduce the ordered spike-and-slab prior in Section 2. The model for the parametric and nonparametric functions, including the constraints, is in Section 3. The MCMC algorithm is discussed in Section 4. A simulation study is in Section 5. The model is applied to real datasets in Section 6. We conclude in Section 7. Online supplementary material includes the full MCMC algorithm, additional simulation results, and R code to reproduce the results in the paper.

2 Ordered spike-and-slab priors

The SFFM (1) augments the parametric template \mathcal{H}_0 with a nonparametric component to reduce bias and model misspecification. These additional terms increase model complexity and should be removed whenever the added complexity is not supported by the data. This effort is related to rank selection, which seeks to identify a small number of necessary factors, yet is complicated by the presence of the parametric template with unknown $\{\alpha_{\ell,i}\}$ and γ .

Leveraging the Bayesian framework, we design an ordered spike-and-slab prior for the nonparametric factors $\{\beta_{k,i}\}$. The spike-and-slab formulation provides joint shrinkage and selection for each $\boldsymbol{\beta}_k = (\beta_{k,1}, \dots, \beta_{k,n})'$ and therefore removes unnecessary nonparametric factors from the model. We build upon the spike-and-slab prior of Ishwaran and Rao (2005) for linear regression and extend this approach to the functional data setting. Compared to linear regression, model (1) is complicated significantly by the infinite-dimensional basis expansion. Our solution is to impose ordering in the spike-and-slab prior. Since additional factors are increasingly pulled toward the spike (inactive) component *a priori*, the posterior distribution is encouraged to concentrate on finite truncations of (1).

2.1 Cumulative shrinkage processes for ordered selection

To incorporate ordered shrinkage and selection into model (1), we build upon the *cumulative shrinkage process* (CSP) proposed by Legramanti et al. (2020). CSPs are sparsity-inducing priors for infinite sequences of parameters with a defined ordering. Suppose that the inclusion of the k th factor β_k is determined by a parameter θ_k ; we provide additional details on our specification of θ_k in Section 2.2. In the general case, CSPs define a spike-and-slab prior for parameters $\{\theta_k\}_{k=1}^\infty$ with a particular structure on the spike probabilities $\{\pi_k\}_{k=1}^\infty$:

$$[\theta_k | \pi_k] \sim P_k, \quad P_k = (1 - \pi_k)P_{slab} + \pi_k P_{spike} \quad (3)$$

$$\pi_k = \sum_{h=1}^k \omega_h, \quad \omega_h = \nu_h \prod_{\ell=1}^{h-1} (1 - \nu_\ell), \quad \nu_\ell \stackrel{iid}{\sim} \text{Beta}(1, K_0), \quad (4)$$

where P_{slab} is distribution of the slab (active) component and P_{spike} is the distribution of the spike (inactive) component. The hyperparameters of the CSP are determined by the distributions P_{slab} and P_{spike} and the scalar $K_0 > 0$, which corresponds to the prior expected number of active components (see (6) below). Legramanti et al. (2020) restrict $P_{spike} = \delta_{\theta_\infty}$ to be a point mass at some pre-specified value θ_∞ ; we consider an alternative approach tailored for model (1) in Section 2.2, and allow P_{spike} to be more general in the subsequent discussions and results. The stick-breaking construction in (4), most commonly used for Dirichlet processes (Ishwaran and James, 2001), ensures an increasing sequence of (spike) probabilities, $\pi_k < \pi_{k+1}$, that converges: $\lim_{k \rightarrow \infty} \pi_k = 1$. Most important, CSPs place increasing prior mass on the spike component as k grows—without imposing an upper bound.

The ordering of the spike probabilities $\{\pi_k\}_{k=1}^\infty$ in (4) implies a certain ordering for the prior distribution of the parameters $\{\theta_k\}_{k=1}^\infty$ in (3), which we formalize in the following result:

Proposition 1. *For $\varepsilon > 0$ and fixed θ_0 , let $\mathbb{B}_\varepsilon(\theta_0) = \{\theta_k : |\theta_k - \theta_0| < \varepsilon\}$. For θ_k with prior*

(3)-(4), we have

$$\mathbb{P}(|\theta_k - \theta_0| \leq \varepsilon) < \mathbb{P}(|\theta_{k+1} - \theta_0| \leq \varepsilon)$$

whenever $P_{slab}\{\mathbb{B}_\varepsilon(\theta_0)\} < P_{spike}\{\mathbb{B}_\varepsilon(\theta_0)\}$.

Proof. The proof proceeds directly:

$$\begin{aligned} \mathbb{P}(|\theta_k - \theta_0| \leq \varepsilon) &= \mathbb{E}[P_k\{\mathbb{B}_\varepsilon(\theta_0)\}] = \mathbb{E}[(1 - \pi_k)P_{slab}\{\mathbb{B}_\varepsilon(\theta_0)\} + \pi_k P_{spike}\{\mathbb{B}_\varepsilon(\theta_0)\}] \\ &= \mathbb{E}\{(1 - \pi_k)\}P_{slab}\{\mathbb{B}_\varepsilon(\theta_0)\} + \mathbb{E}(\pi_k)P_{spike}\{\mathbb{B}_\varepsilon(\theta_0)\} \\ &= P_{slab}\{\mathbb{B}_\varepsilon(\theta_0)\}\{K_0/(1 + K_0)\}^k + P_{spike}\{\mathbb{B}_\varepsilon(\theta_0)\}[1 - \{K_0/(1 + K_0)\}^k] \\ &= P_{spike}\{\mathbb{B}_\varepsilon(\theta_0)\} + \{K_0/(1 + K_0)\}^k[P_{slab}\{\mathbb{B}_\varepsilon(\theta_0)\} - P_{spike}\{\mathbb{B}_\varepsilon(\theta_0)\}] \end{aligned}$$

noting $\mathbb{E}(\pi_k) = 1 - \{K_0/(1 + K_0)\}^k$ (Legramanti et al., 2020). Since $\{K_0/(1 + K_0)\}^k \in [0, 1]$ is decreasing in k and the remaining terms are invariant to k , the result follows. \square

Intuitively, for any θ_0 that is favored under the spike distribution P_{spike} relative to the slab distribution P_{slab} , the CSP prior (3)-(4) places greater mass around θ_0 as k increases. For spike-and-slab priors, we are most interested in $\theta_0 = 0$. The special case of Proposition 1 with $P_{spike} = \delta_{\theta_\infty}$ and $\theta_0 = 0$ is proved by Legramanti et al. (2020).

For interpretability and efficient MCMC sampling, there is a convenient data augmentation of the CSP prior (3). Let $z_k \in \{1, \dots, \infty\}$ denote a categorical variable with $\mathbb{P}(z_k = h|\omega_h) = \omega_h$. The specification

$$[\theta_k|z_k] \sim (1 - \mathbb{I}\{z_k \leq k\})P_{slab} + \mathbb{I}\{z_k \leq k\}P_{spike} \quad (5)$$

induces (3) via marginalization over z_k . The number of active (slab) terms is therefore

$$K^* = \sum_{k=1}^{\infty} \mathbb{I}\{z_k > k\} \quad (6)$$

for which posterior inference is available through the proposed MCMC sampling algorithm (see Algorithm 1). For model (1), K^* is the effective number of nonparametric terms, and therefore is an important inferential target to assess the adequacy of the parametric model.

The prior expected number of slab terms is $\mathbb{E}(K^*) = K_0$, which appears in (4) and allows for the inclusion of prior information regarding the number of factors. The choice of K_0 can influence the posterior distribution for K^* , and thus subsequent inference on the number of nonparametric factors in (1). To mitigate this effect, we propose the hyperprior $K_0 \sim \text{Gamma}(a_{K_0}, b_{K_0})$ for $a_{K_0}, b_{K_0} > 0$, which is conditionally conjugate to (4). The hyperparameters may be selected to provide weak prior information regarding the number of factors: in practice, we set $a_{K_0} = 2$ and $b_{K_0} = 1$ so that $\mathbb{E}(K_0) = \text{Var}(K_0) = 2$.

2.2 Parameter-expanded spike-and-slab models

The CSP prior provides an appealing mechanism for introducing ordered shrinkage and selection into model (1). To do so, we parametrize the prior for the factors $\{\beta_{k,i}\}$ in terms of $\{\theta_k\}$ in (3). A subtle yet important feature of this framework is that spike-and-slab selection is applied jointly to the entire n -dimensional *vector* $\beta_k = (\beta_{k,1}, \dots, \beta_{k,n})'$. However, parametrization of a vector β_k in terms of a spike-and-slab prior on a scalar θ_k is known to introduce significant challenges for MCMC sampling. Scheipl et al. (2012) show that as the dimension of the parameter vector increases, it becomes increasingly more difficult for the MCMC algorithm to escape local basins of attraction, or more specifically, to switch between the slab and spike components. The consequences are nontrivial: without the ability to traverse between the slab and spike components, the uncertainty quantification for each factor's activeness is invalidated, and inference for the effective number of nonparametric factors K^* cannot proceed.

To illustrate, we compare the proposed approach to Legramanti et al. (2020), which uses CSP priors but does not address this issue. We simulate $n = 100$ curves each with $m = 50$

observation points using a linear template with $K_{true} = 5$ additional nonparametric factors (see Section 5). The analogous prior in Legramanti et al. (2020) is $[\beta_{k,i}|\theta_k] \stackrel{indep}{\sim} N(0, \theta_k)$ and a CSP prior for $\{\theta_k\}_{k=1}^\infty$ with $P_{spike} = \delta_{\theta_\infty}$ and $P_{slab} = \text{Inv-Gamma}(a_\theta, b_\theta)$. We use the hyperparameters from Legramanti et al. (2020): $\theta_\infty = 0.05$ and $a_\theta = b_\theta = 2$, but the subsequent results persist for other choices. Since Legramanti et al. (2020) treat K_0 as fixed, we set it to the true value, $K_0 = 5$.

Figure 2 displays the MCMC samples of K^* across five different MCMC runs with random initializations. The proposed approach produces draws that are centered at the true value with some variability: K^* changes values in 27% of the MCMC iterations. By comparison, the Legramanti et al. (2020) prior and sampler produces MCMC draws that are essentially stuck at a single value: K^* changes values in only 0.01% of the MCMC iterations. Clearly, the latter results cannot be used to provide reliable posterior uncertainty quantification for the effective number of nonparametric components K^* . Further, the proposed approach is more accurate: we estimate $\mathbb{E}(K^*|\mathbf{y}) = 4.9$ for the proposed approach and $\mathbb{E}(K^*|\mathbf{y}) = 3.9$ for the Legramanti et al. (2020) prior.

Our solution is to introduce a redundant parameter expansion for the ordered spike-and-slab prior. The utility of redundant parameter expansions for improved MCMC mixing was explored in Gelman (2006) for variance parameters in hierarchical models. In the context of spike-and-slab priors, parameter expansions have proven useful for function selection in additive models (Scheipl et al., 2012) and lag selection in functional autoregression models Kowal et al. (2017b), and in both cases provide adequate uncertainty quantification for posterior inclusion probabilities.

We induce a prior on each factor $\beta_{k,i}$ via the following parameter expansion:

$$\beta_{k,i} = \eta_k \xi_{k,i} \tag{7}$$

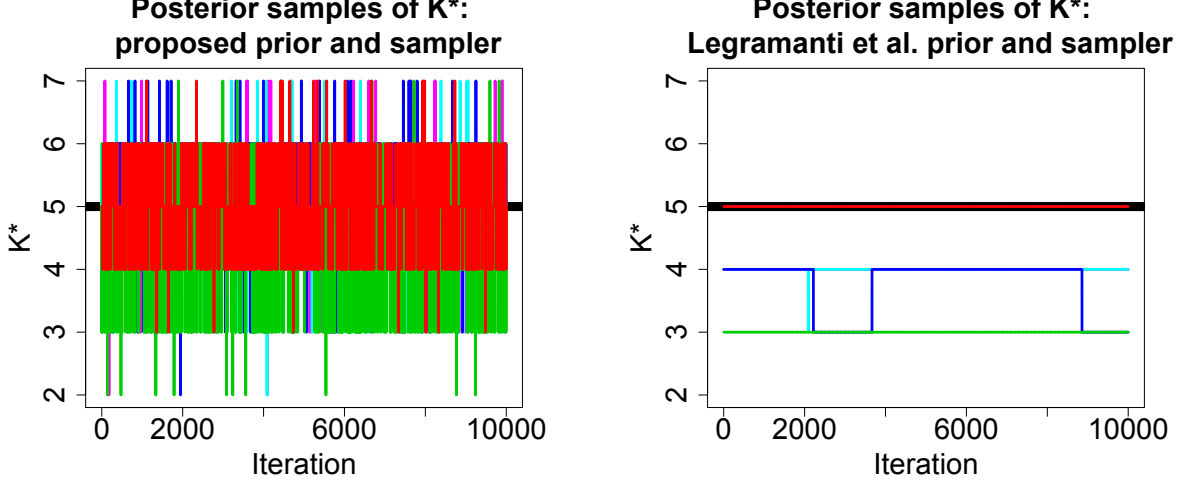


Figure 2: MCMC samples of K^* across 5 chains for the proposed prior and algorithm (left) compared to Legramanti et al. (2020) (right). The horizontal black line denotes the true value $K_{true} = 5$. The proposed approach provides substantial improvements in mixing and produces more accurate estimates.

where η_k applies the ordered spike-and-slab shrinkage for factor k and $\{\xi_{k,i}\}_{i=1}^n$ disperses this shrinkage throughout $\{\beta_{k,i}\}_{i=1}^n$. Here, $\xi_{k,i}$ is nonidentifiable and exists primarily for the purpose of improving MCMC performance. The spike-and-slab structure in the prior is introduced via a normal mixture of inverse-gamma (NMIG) prior on the scalars η_k :

$$[\eta_k | \theta_k, \sigma_k^2] \stackrel{indep}{\sim} N(0, \theta_k \sigma_k^2) \quad (8)$$

$$[\theta_k | \pi_k] \sim (1 - \pi_k) \delta_1 + \pi_k \delta_{v_0} \quad (9)$$

$$[\sigma_k^{-2}] \stackrel{iid}{\sim} \text{Gamma}(a_1, a_2) \quad (10)$$

where v_0 , a_1 and a_2 are hyperparameters. The NMIG prior of Ishwaran and Rao (2005) incorporates variable selection by assigning the variance scale parameter θ_k to the slab component, $\theta_k = 1$, or the spike component, $\theta_k = v_0$. By design, the NMIG prior produces a continuous distribution for the conditional variance of η_k , which is shown by Ishwaran and Rao (2005) to be preferable for variable selection and risk properties. Further, Ishwaran and

Rao (2005) and Scheipl et al. (2012) note that the NMIG prior is less sensitive to hyper-parameter choices compared to other spike-and-slab priors (O’Hara and Sillanpää, 2009), which mitigates a fundamental challenge in these models.

The parameter-expansion terms are assigned the prior

$$[\xi_{k,i}|m_{\xi_{k,i}}] \stackrel{indep}{\sim} N(m_{\xi_{k,i}}, 1), \quad m_{\xi_{k,i}} \stackrel{indep}{\sim} \frac{1}{2}\delta_1 + \frac{1}{2}\delta_{-1} \quad (11)$$

and (7)-(11) is referred to as the parameter-expanded NMIG (peNMIG) prior (Scheipl et al., 2012). The Gaussian parameter expansion of $\xi_{k,i}$ resembles Gelman (2006), yet is centered around 1 or -1 with variance 1. As a result, the parameter η_k retains the interpretability as a selection parameter and assigns the magnitude to β_k .

The key distinction between the proposed prior and the peNMIG prior of Scheipl et al. (2012) is the ordering implied by the prior for $\{\pi_k\}_{k=1}^\infty$ given in (4). Direct application of Scheipl et al. (2012), in which the π_k probabilities in (9) are common for all k and assigned a Beta prior, is not appropriate for model (1): that approach does not provide ordered shrinkage or selection and is not designed to accommodate growing model dimension with an implicit ordering. Consider the marginal prior for η_k in (8)-(10), conditional on π_k :

$$[\eta_k|\pi_k] \sim (1 - \pi_k)t_{2a_1}(0, \sqrt{a_2/a_1}) + \pi_k t_{2a_1}(0, \sqrt{v_0 a_2/a_1}) \quad (12)$$

where $t_d(m, s)$ denotes a t -distribution with mean m , standard deviation s , and degrees of freedom d . By coupling (12) with the CSP prior for $\{\pi_k\}$ in (4), we obtain the following ordering result for the marginal prior on $\{\eta_k\}_{k=1}^\infty$ (unconditional on π_k):

Corollary 1. *For $\varepsilon > 0$, $\mathbb{P}(|\eta_k| \leq \varepsilon) < \mathbb{P}(|\eta_{k+1}| \leq \varepsilon)$ whenever $v_0 < 1$.*

Corollary 1 follows from Proposition 1 by observing that (12) is a special case of (3) and that the densities of the t -distributions in (3) place greater mass near zero when the scale

parameter is smaller. The restriction $v_0 < 1$ is self-evident, since it ensures that the spike distribution is indeed more concentrated around zero.

This crucial ordering maintains for the parameter-expanded prior induced by (7):

Proposition 2. *For $\varepsilon > 0$, $\mathbb{P}(|\beta_{k,i}| \leq \varepsilon) < \mathbb{P}(|\beta_{k+1,i}| \leq \varepsilon)$ whenever $v_0 < 1$.*

Proof. Since $\{\xi_{k,i}\}$ are iid (upon marginalization over $\{m_{\xi_{k,i}}\}$), it follows that $\mathbb{P}(|\beta_{k,i}| \leq \varepsilon) = \mathbb{P}(|\eta_k \xi_{k,i}| \leq \varepsilon) = \mathbb{P}(|\eta_k \xi_{k+1,i}| \leq \varepsilon)$. Then we proceed directly:

$$\begin{aligned} \mathbb{P}(|\beta_{k,i}| \leq \varepsilon) &= \mathbb{P}(|\eta_k \xi_{k+1,i}| \leq \varepsilon) = \mathbb{E}\{\mathbb{I}(|\eta_k| |\xi_{k+1,i}| \leq \varepsilon)\} \\ &= \mathbb{E}[\mathbb{E}\{\mathbb{I}(|\eta_k| |\xi_{k+1,i}| \leq \varepsilon) | \xi_{k+1,i}\}] \\ &= \mathbb{E}[\mathbb{P}(|\eta_k| |\xi_{k+1,i}| \leq \varepsilon | \xi_{k+1,i})] \\ &< \mathbb{E}[\mathbb{P}(|\eta_{k+1}| |\xi_{k+1,i}| \leq \varepsilon | \xi_{k+1,i})] \\ &= \mathbb{P}(|\beta_{k+1,i}| \leq \varepsilon), \end{aligned}$$

where the inequality follows from Corollary 1. □

Proposition 2 requires only that $\{\xi_{k,i}\}$ are marginally independent and identically distributed. Therefore, other parameter-expansion schemes may be substituted in (7) without disrupting the probabilistic ordering of $|\beta_{k,i}|$. By a similar argument, the ordering also is preserved across observations: $\mathbb{P}(|\beta_{k,i}| \leq \varepsilon) < \mathbb{P}(|\beta_{k+1,i'}| \leq \varepsilon)$ for $\varepsilon > 0$ and $v_0 < 1$.

For practical implementation, it is advantageous to truncate the infinite summation in (1), which provides simpler and faster computations. The following result shows that finite approximations are accurate for sufficiently large truncation K :

Proposition 3. *Let $\theta^{(K)} = \{\theta_k\}_{k=1}^K$ denote the sequence $\{\theta_k\}_{k=1}^\infty$ truncated at K . For $0 < v_0 < \varepsilon < 1$, we have $\mathbb{P}\{d_\infty(\theta, \theta^{(K)}) > \varepsilon\} \leq K_0\{K_0/(1 + K_0)\}^K$.*

Proof. For the prior (9), note that $P_{slab} = \delta_1$ and $P_{spike} = \delta_{v_0}$, so $P_{slab}\{\bar{\mathbb{B}}_\varepsilon(0)\} = 1$ if $\varepsilon < 1$ and $P_{spike}\{\bar{\mathbb{B}}_\varepsilon(0)\} = 0$ if $\varepsilon > v_0$, where $\bar{\mathbb{B}}_\varepsilon(0)$ denotes the complement of $\mathbb{B}_\varepsilon(0)$. Using the proof

of Proposition 1, we have $\mathbb{P}\{d_\infty(\theta, \theta^{(K)}) > \varepsilon\} = \mathbb{P}\{\sup_{k>K} |\theta_k| > \varepsilon\} \leq \sum_{k>K} \mathbb{P}(|\theta_k| > \varepsilon) = \sum_{k>K} \{K_0/(1+K_0)\}^k = K_0\{K_0/(1+K_0)\}^K$. \square

The approximation error induced by truncating $\{\theta_k\}_{k=1}^\infty$ to K terms decreases rapidly in K , which suggests that the proposed infinite-dimensional ordered spike-and-slab prior is accurately approximated by a conservative truncation. Since we obtain inference for the effective number of active components, K^* , we can assess whether the posterior distribution of K^* places mass on values near K , which indicates that a larger value of K is necessary.

3 Models and constraints for the basis functions

3.1 Model for the nonparametric functions

The error-free latent functions $\{Y_i\}$ belong to the space spanned by the template parametric curves $\{g_\ell\}$ and the nonparametric curves $\{f_k\}$. Any systemic bias resulting from the inadequacies of $\{g_\ell\}$ must be corrected by $\{f_k\}$, which demands substantial flexibility of the nonparametric basis $\{f_k\}$. However, interpretability of the parametric terms $\{g_\ell\}$ and $\{\alpha_{\ell,i}\}$ requires a strict distinction between the parametric and nonparametric components.

To achieve both flexibility and distinctness, we model each f_k as a smooth unknown function such that each f_k is orthogonal to $\{g_\ell\}$. The model for f_k can be any Bayesian curve-fitting model, such as splines, wavelets, or Gaussian processes, usually with a prior that encourages smoothness. The orthogonality constraints ensure nonredundancy of $\{f_k\}$ and offer key computational simplifications that improve scalability and increase MCMC efficiency. These results maintain regardless of the specification of $\{g_\ell\}$ or $\{f_k\}$.

Let $f_k(\tau) = \mathbf{b}'(\tau)\boldsymbol{\psi}_k$ be a linear combination of known basis functions \mathbf{b} and unknown coefficients $\boldsymbol{\psi}_k$. We use low-rank thin plate splines for \mathbf{b} , which are flexible, computationally efficient, and well-defined on $\mathcal{T} \subset \mathbb{R}^d$ for $d \in \mathbb{Z}^+$, and have demonstrated exceptional mod-

eling performance in related functional data problems (Kowal, 2019; Kowal and Bourgeois, 2020). The prior on each vector of basis coefficients $\boldsymbol{\psi}_k$ is specified to encourage smoothness of f_k , akin to a classical spline roughness penalty:

$$[\boldsymbol{\psi}_k | \lambda_{f_k}] \stackrel{indep}{\sim} N(\mathbf{0}, \lambda_{f_k}^{-1} \boldsymbol{\Omega}^-), \quad \lambda_{f_k}^{-1/2} \stackrel{indep}{\sim} \text{Uniform}(0, 10^4), \quad (13)$$

where $\lambda_{f_k} > 0$ is the prior precision and $\boldsymbol{\Omega}$ is a known (roughness) penalty matrix. We select $\boldsymbol{\Omega}$ to be the matrix of integrated squared second derivatives, $[\boldsymbol{\Omega}]_{j,j'} = \int \ddot{b}_j(\tau) \ddot{b}_{j'}(\tau) d\tau$, which implies that the prior distribution satisfies $-2 \log p(\boldsymbol{\psi}_k | \lambda_{f_k}) \stackrel{c}{=} \lambda_{f_k} \boldsymbol{\psi}_k' \boldsymbol{\Omega} \boldsymbol{\psi}_k = \lambda_{f_k} \int \{\ddot{f}_k(\tau)\}^2 d\tau$ and $\stackrel{c}{=}$ denotes equality up to a constant. The prior operates as a roughness penalty with an unknown smoothing parameter λ_{f_k} that is learned from the data. For more convenient and efficient computing, standard reparametrizations can diagonalize the penalty matrix $\boldsymbol{\Omega}$ and orthogonalize the basis matrix $\mathbf{B} = (\mathbf{b}'(\tau_1), \dots, \mathbf{b}'(\tau_m))'$ (Kowal, 2020). Details on low-rank thin plate splines and generalizations for $d > 1$ are given in Wood (2006).

The full conditional distributions of the nonparametric basis coefficients $\boldsymbol{\psi}_k$ are derived in Section 3.3. Importantly, these distributions incorporate key orthogonality constraints, which are motivated and described in the following section.

3.2 Orthogonality of the parametric and nonparametric functions

Orthogonality of the joint basis $\{g_1, \dots, g_L, f_1, f_2, \dots\}$ is decomposed into three sets of constraints: orthogonality of the parametric basis $\{g_\ell\}_{\ell=1}^L$, orthogonality of the nonparametric basis $\{f_k\}_{k=1}^\infty$, and orthogonality between each parametric function g_ℓ and nonparametric function f_k . Consider model (1)-(2) evaluated at the observation points $\{\tau_j\}_{j=1}^m$:

$$\mathbf{y}_i = \mathbf{G}_\gamma \boldsymbol{\alpha}_i + \mathbf{F} \boldsymbol{\beta}_i + \boldsymbol{\epsilon}_i, \quad \boldsymbol{\epsilon}_i \stackrel{indep}{\sim} N(\mathbf{0}, \sigma_\epsilon^2 \mathbf{I}_m), \quad i = 1, \dots, n \quad (14)$$

where $\boldsymbol{\alpha}_i = (\alpha_{1,i}, \dots, \alpha_{L,i})'$, $\mathbf{F} = (\mathbf{f}_1, \dots, \mathbf{f}_K)$ for $\mathbf{f}_k = (f_k(\tau_1), \dots, f_k(\tau_m))' = \mathbf{B}\boldsymbol{\psi}_k$, and $\boldsymbol{\beta}_i = (\beta_{1,i}, \dots, \beta_{K,i})'$. Here, we have truncated the CSP prior at some conservative upper bound K as justified by Proposition 3.

The parametric matrix \mathbf{G}_γ is constructed and orthogonalized using a QR decomposition. For any value of γ , let $\mathbf{G}_\gamma^0 = \mathbf{Q}_\gamma \mathbf{R}_\gamma$ be the QR decomposition of the initial basis matrix $\mathbf{G}_\gamma^0 = (\mathbf{g}_{1;\gamma}, \dots, \mathbf{g}_{L;\gamma})$ with $\mathbf{g}_{\ell;\gamma} = (g_\ell(\tau_1; \gamma), \dots, g_\ell(\tau_m; \gamma))'$. By setting $\mathbf{G}_\gamma = \mathbf{Q}_\gamma$, we ensure that $\mathbf{G}_\gamma' \mathbf{G}_\gamma = \mathbf{I}_L$ and the columns of \mathbf{G}_γ span the same space as the columns of \mathbf{G}_γ^0 . When γ is unknown and endowed with a prior distribution, the QR decomposition is incorporated into the likelihood evaluations of (14) for posterior sampling of γ .

The nonparametric basis matrix \mathbf{F} is constrained such that $\mathbf{F}' \mathbf{F} = \mathbf{I}_K$ and $\mathbf{G}_\gamma' \mathbf{F} = \mathbf{0}_{L \times K}$. The latter constraint is vital, and factors the likelihood (14) into parametric and nonparametric terms:

Lemma 1. *When $\mathbf{G}_\gamma' \mathbf{F} = \mathbf{0}_{L \times K}$, the likelihood (14) factorizes: $p(\mathbf{y}|\gamma, \{\boldsymbol{\alpha}_i\}, \mathbf{F}, \{\boldsymbol{\beta}_i\}, \sigma_\epsilon^2) = p_0(\mathbf{y}|\gamma, \{\boldsymbol{\alpha}_i\}, \sigma_\epsilon^2) p_1(\mathbf{y}|\mathbf{F}, \{\boldsymbol{\beta}_i\}, \sigma_\epsilon^2)$, where p_0 depends on the parametric terms, γ and $\{\boldsymbol{\alpha}_i\}$, and the error variance σ_ϵ^2 , and p_1 depends on the nonparametric terms, \mathbf{F} and $\{\boldsymbol{\beta}_i\}$, and σ_ϵ^2 .*

Within a Bayesian model, a reasonable notion of distinctness between parametric and nonparametric components is (conditional) independence in the posterior. By assuming independence in the prior, Lemma 1 ensures this result:

Corollary 2. *Suppose the parametric and nonparametric factors are a priori independent: $p(\{\boldsymbol{\alpha}_i\}, \{\boldsymbol{\beta}_i\}) = p(\{\boldsymbol{\alpha}_i\})p(\{\boldsymbol{\beta}_i\})$. Under model (14) and subject to $\mathbf{G}_\gamma' \mathbf{F} = \mathbf{0}_{L \times K}$, the parametric and nonparametric factors are a posteriori independent, $p(\{\boldsymbol{\alpha}_i\}, \{\boldsymbol{\beta}_i\}|\mathbf{y}, \sigma_\epsilon^2, \mathbf{F}, \gamma) = p(\{\boldsymbol{\alpha}_i\}|\mathbf{y}, \sigma_\epsilon^2, \mathbf{F}, \gamma) p(\{\boldsymbol{\beta}_i\}|\mathbf{y}, \sigma_\epsilon^2, \mathbf{F}, \gamma)$, conditional on $\sigma_\epsilon^2, \mathbf{F}, \gamma$.*

The consequences of Corollary 2 are important for posterior inference: by constraining the unknown nonparametric curves \mathbf{F} to be orthogonal to \mathbf{G}_γ , we ensure that the sampling steps for all parametric factors $\{\boldsymbol{\alpha}_i\}$ do *not* depend on the nonparametric parameters in any

way. In particular, the sampling steps for $\{\boldsymbol{\alpha}_i\}$ are identical to the fully parametric case, while the sampling steps for $\{\boldsymbol{\beta}_i\}$ proceed exactly as in a fully nonparametric setting (see Algorithm 1). This decoupling of parametric and nonparametric sampling steps is crucial for accommodating increases in model complexity.

3.3 Enforcing the orthogonality constraints

For each f_k , the orthogonality constraints are enforced in two stages: (i) the linear constraints $\mathbf{G}'_\gamma \mathbf{f}_k = \mathbf{0}_L$ and $\mathbf{f}'_{k'} \mathbf{f}_k = 0$ for $k' \neq k$ are *conditioned upon* and (ii) the unit norm constraint $\mathbf{f}'_k \mathbf{f}_k = 1$ is satisfied via normalization after sampling. Alternative approaches that directly sample from the Stiefel manifold are available (Jauch et al., 2019), yet require customized algorithms and modifications to accommodate the additional constraint $\mathbf{G}'_\gamma \mathbf{f}_k = \mathbf{0}_L$.

Under the prior (13) and the likelihood (14), the full conditional posterior distribution for each $\boldsymbol{\psi}_k$ is $N(\mathbf{Q}_{\boldsymbol{\psi}_k}^{-1} \boldsymbol{\ell}_{\boldsymbol{\psi}_k}, \mathbf{Q}_{\boldsymbol{\psi}_k}^{-1})$ for $k = 1, \dots, K$, where $\mathbf{Q}_{\boldsymbol{\psi}_k} = \sigma_\epsilon^{-2} (\mathbf{B}' \mathbf{B}) \sum_{i=1}^n \beta_{k,i}^2 + \lambda_{f_k} \boldsymbol{\Omega}$ and $\boldsymbol{\ell}_{\boldsymbol{\psi}_k} = \sigma_\epsilon^{-2} \mathbf{B}' \sum_{i=1}^n \{\beta_{k,i} (\mathbf{y}_i - \mathbf{G}_\gamma \boldsymbol{\alpha}_i - \sum_{\ell \neq k} \mathbf{f}_\ell \beta_{\ell,i})\}$. Jointly, we represent the linear constraints on the basis coefficients as $\mathbf{C}_k \boldsymbol{\psi}_k = \mathbf{0}$, where $\mathbf{C}_k = (\mathbf{G}_\gamma, \mathbf{f}_1, \dots, \mathbf{f}_{k-1}, \mathbf{f}_{k+1}, \dots, \mathbf{f}_K)' \mathbf{B}$. The constraint is linear in $\boldsymbol{\psi}_k$; conditioning on this constraint produces another Gaussian distribution. Samples from this distribution are easy to obtain: given a draw $\boldsymbol{\psi}_k^0 \sim N(\mathbf{Q}_{\boldsymbol{\psi}_k}^{-1} \boldsymbol{\ell}_{\boldsymbol{\psi}_k}, \mathbf{Q}_{\boldsymbol{\psi}_k}^{-1})$ from the unconstrained full conditional distribution, the vector $\boldsymbol{\psi}_k = \boldsymbol{\psi}_k^0 - \mathbf{Q}_{\boldsymbol{\psi}_k}^{-1} \mathbf{C}_k' (\mathbf{C}_k \mathbf{Q}_{\boldsymbol{\psi}_k}^{-1} \mathbf{C}_k')^{-1} \mathbf{C}_k \boldsymbol{\psi}_k^0$ constitutes a draw from the full conditional distribution subject to the orthogonality constraints (Kowal, 2020). After drawing $\boldsymbol{\psi}_k$, we rescale both $\boldsymbol{\psi}_k$ and $\beta_{k,i}$ to enforce the unit-norm constraint while preserving the product $\mathbf{f}_k \beta_{k,i}$ in the likelihood (14): we set $\beta_{k,i} \rightarrow \beta_{k,i} \|\mathbf{B} \boldsymbol{\psi}_k\|$ and $\boldsymbol{\psi}_k \rightarrow \boldsymbol{\psi}_k \|\mathbf{B} \boldsymbol{\psi}_k\|$ and then let $\mathbf{f}_k = \mathbf{B} \boldsymbol{\psi}_k$. This operation does not change the shape of the curve f_k nor the likelihood (14). Most important, the constraints $\mathbf{G}'_\gamma \mathbf{F} = \mathbf{0}_{L \times K}$ and $\mathbf{F}' \mathbf{F} = \mathbf{I}_K$ hold at every MCMC iteration.

4 MCMC for posterior inference

We design an efficient MCMC algorithm for posterior inference. The efficiency of the algorithm derives from two key features: the parameter-expanded sampler for the ordered spike-and-slab prior, which substantially improves MCMC mixing (see Figure 2), and the orthogonality constraints on $\{g_\ell\}$ and $\{f_k\}$, which produce important computational simplifications. The full MCMC algorithm is detailed in the supplementary material.

Algorithm 1 presents the sampling steps for the ordered spike-and-slab parameters. These steps consist of simple, fast, and closed form updates. The full conditionals depend on the data only through $y_{k,i}^F = \mathbf{f}_k' \mathbf{y}_i$, which offers an implicit dimension reduction from m to K and does not involve the parametric terms. These simplifications are a direct consequence of the orthogonality constraints. In addition, we retain posterior samples of $K^* = \sum_{k=1}^K \mathbb{I}\{z_k > k\}$, which is the effective number of nonparametric terms. Adaptations of this sampling algorithm for use of the ordered spike-and-slab prior with other models, such as (non-functional) factor models, are available by replacing $y_{k,i}^F$ with the appropriate term.

The sampling steps for the nonparametric functions $\{\mathbf{f}_k\}$ subject to orthogonality constraints are discussed in Section 3.3. Here, we note that these constraints pay dividends for efficient sampling of the parametric factors. Consider the prior $\alpha_{\ell,i} \stackrel{indep}{\sim} N(0, \sigma_{\alpha_\ell}^2)$; alternative priors (see Section 6.2) benefit similarly. The full conditional distribution is simply $[\boldsymbol{\alpha}_i | -] \stackrel{indep}{\sim} N(\mathbf{Q}_{\alpha_i}^{-1} \boldsymbol{\ell}_{\alpha_i}, \mathbf{Q}_{\alpha_i}^{-1})$ for $i = 1, \dots, n$, where $\mathbf{Q}_{\alpha_i} = \sigma_\epsilon^{-2} \mathbf{I}_L + \text{diag}(\{\sigma_{\alpha_\ell}^{-2}\}_{\ell=1}^L)$ and $\boldsymbol{\ell}_{\alpha_i} = \sigma_\epsilon^{-2} \mathbf{G}_\gamma' \mathbf{y}_i$. The parametric factors are conditionally independent and do not involve any of the nonparametric terms, and therefore can be sampled jointly and efficiently.

5 Simulation study

We conduct a simulation study to assess model performance for (i) point and interval prediction of Y_i and \mathbf{y}_i , (ii) estimation and inference for the parametric coefficients $\{\boldsymbol{\alpha}_i\}$, and (iii)

Algorithm 1: MCMC sampling steps for the ordered spike-and-slab prior

Let $y_{k,i}^F = \mathbf{f}_k' \mathbf{y}_i$ for $i = 1, \dots, n$ and $k = 1, \dots, K$:

1. **Sample** $[m_{\xi_{k,i}} | -]$ from $\{-1, 1\}$ with $\mathbb{P}(m_{\xi_{k,i}} = 1 | -) = 1 / \{1 + \exp(-2\xi_{h,i})\}$;
2. **Sample** $[\xi_{k,i} | -] \sim N(Q_{\xi_{k,i}}^{-1} \ell_{\xi_{k,i}}, Q_{\xi_{k,i}}^{-1})$ where $Q_{\xi_{k,i}} = \eta_k^2 / \sigma_\epsilon^2 + 1$ and $\ell_{\xi_{k,i}} = \eta_k y_{k,i}^F / \sigma_\epsilon^2 + m_{\xi_{k,i}}$;
3. **Sample** $[\eta_k | -] \sim N(Q_{\eta_k}^{-1} \ell_{\eta_k}, Q_{\eta_k}^{-1})$ where $Q_{\eta_k} = \sum_{i=1}^n \xi_{k,i}^2 / \sigma_\epsilon^2 + (\theta_k \sigma_k^2)^{-1}$ and $\ell_{\eta_k} = \sum_{i=1}^n \xi_{k,i} y_{k,i}^F / \sigma_\epsilon^2$;
4. **Rescale** $\eta_k \rightarrow (\sum_{i=1}^n |\xi_{k,i}| / n) \eta_k$ and $\boldsymbol{\xi}_k \rightarrow (n / \sum_{i=1}^n |\xi_{k,i}|) \boldsymbol{\xi}_k$ and **update** $\beta_{k,i} = \xi_{k,i} \eta_k$;
5. **Sample** $[\sigma_k^{-2} | -] \sim \text{Gamma}\{a_1 + 1/2, a_2 + \eta_k^2 / (2\theta_k)\}$;
6. **Sample** $[\nu_k | -] \sim \text{Beta}(1 + \sum_{h=1}^K \mathbb{I}\{z_h = k\}, K_0 + \sum_{h=1}^K \mathbb{I}\{z_h > k\})$ for $k = 1, \dots, K-1$ and **update** π_k and ω_k from (4);
7. **Sample** $[K_0 | -] \sim \text{Gamma}\{a_{K_0} + K - 1, b_{K_0} - \sum_{k=1}^{K-1} \log(1 - \nu_k)\}$;
8. **Sample** $[z_k | -]$ from

$$\mathbb{P}(z_k = h | -) \propto \begin{cases} \omega_h t_{2a_1}(\eta_k; 0, \sqrt{v_0 a_2 / a_1}) & h \leq k \\ \omega_h t_{2a_1}(\eta_k; 0, \sqrt{a_2 / a_1}) & h > k \end{cases}$$

where $t_d(x; m, s)$ is the density of the t -distribution evaluated at x with mean m , standard deviation s , and degrees of freedom d ;

9. **Update** $\theta_k = 1$ if $z_k > k$ and $\theta_k = v_0$ if $z_k \leq k$.
-

uncertainty quantification for the number of nonparametric terms. We focus on the linear template $\mathcal{H}_0 = \text{span}\{1, \tau\}$ and present results for the Nelson-Siegel template (see Section 6.2) with unknown γ in the supplementary material. Despite the additional complexity of the Nelson-Siegel basis, the results remain consistent with those presented here.

Synthetic functional data with $n = 100$ curves and $m = 25$ equally-spaced observation points in $[0, 1]$ are generated as follows. The parametric and nonparametric factors are simulated as $\alpha_{\ell,i}^* \stackrel{iid}{\sim} N(0, 1)$ and $\beta_{k,i}^* \stackrel{indep}{\sim} N(0, 1/(k+1))$, respectively, for $k = 1, \dots, K_{true}$ and $K_{true} \in \{0, 1, 3\}$. By design, the variability in the parametric factors outweighs the variability in the nonparametric factors. The parametric basis matrix \mathbf{G}_γ^* is constructed by evaluating $\{g_\ell\}$ at each observation point and QR-decomposing the resulting matrix as in Section 3.2.

For the nonparametric functions f_k^* , we use orthogonal polynomials of degree $k + 1$, which are orthogonal to the linear template; the Nelson-Siegel version requires an additional QR-based orthogonalization step. The error-free latent functions are $\mathbf{Y}_i^* = \mathbf{G}_\gamma^* \boldsymbol{\alpha}_i^* + \mathbf{F}^* \boldsymbol{\beta}_i^*$ and the functional observations are generated as $\mathbf{y}_i = \mathbf{Y}_i^* + \sigma^* \boldsymbol{\epsilon}_i^*$ where $\sigma^* = \text{sd}(\mathbf{Y}_i^*)/\text{RSNR}$ for sample standard deviation $\text{sd}(\cdot)$, root signal-to-noise ratio $\text{RSNR} = 5$, and $\boldsymbol{\epsilon}_i^* \stackrel{iid}{\sim} N(\mathbf{0}, \mathbf{I}_m)$. This process was repeated to create 100 synthetic datasets.

For both the PFFM and the SFFM, we assume the conditionally Gaussian likelihood (14) with the hierarchical priors

$$[\alpha_{\ell,i} | \sigma_{\alpha_\ell}] \stackrel{indep}{\sim} N(0, \sigma_{\alpha_\ell}^2), \quad \sigma_{\alpha_\ell} \stackrel{iid}{\sim} C^+(0, 1), \quad p(\sigma_\epsilon^2) \propto 1/\sigma_\epsilon^2, \quad (15)$$

and the SFFM hyperparameters $a_1 = 5$, $a_2 = 25$, and $v_0 = 0.001$, with an upper bound $K = 10$ on the number of nonparametric factors. Sensitivity analyses were conducted for $(a_1, a_2) \in \{(5, 25), (5, 50), (10, 30)\}$ and $v_0 \in \{0.01, 0.005, 0.00025\}$. The results for point and interval predictions and estimates of \mathbf{Y}_i^* and $\{\alpha_{\ell,i}^*\}$ are highly robust to these hyperparameters. Inference on K^* is typically robust with the exception of $v_0 = 0.00025$, for which the posterior of K^* becomes more sensitive to (a_1, a_2) . Hence, we select a larger value of v_0 .

Point prediction accuracy is evaluated using root mean squared prediction error for \mathbf{Y}_i^* based on the posterior expectation of \mathbf{Y}_i in (1). The results are in Figure 3. The point predictions perform similarly when the parametric model is correct ($K_{true} = 0$), yet the PFFM accuracy deteriorates significantly for $K_{true} > 0$. The SFFM is accurate for both $K_{true} = 0$ and $K_{true} > 0$.

The 95% pointwise prediction intervals for the PFFM and the SFFM are evaluated based on interval width and coverage in Figure 4. Specifically, we compute the mean prediction interval widths $(nm)^{-1} \sum_{i=1}^n \sum_{j=1}^m \{y_i^{(U)}(\tau_j) - y_i^{(L)}(\tau_j)\}$ and empirical coverage $(nm)^{-1} \sum_{i=1}^n \sum_{j=1}^m \mathbb{I}\{y_i^*(\tau_j) \in (y_i^{(L)}(\tau_j), y_i^{(U)}(\tau_j))\}$, where $(y_i^{(L)}(\tau_j), y_i^{(U)}(\tau_j))$ is the prediction

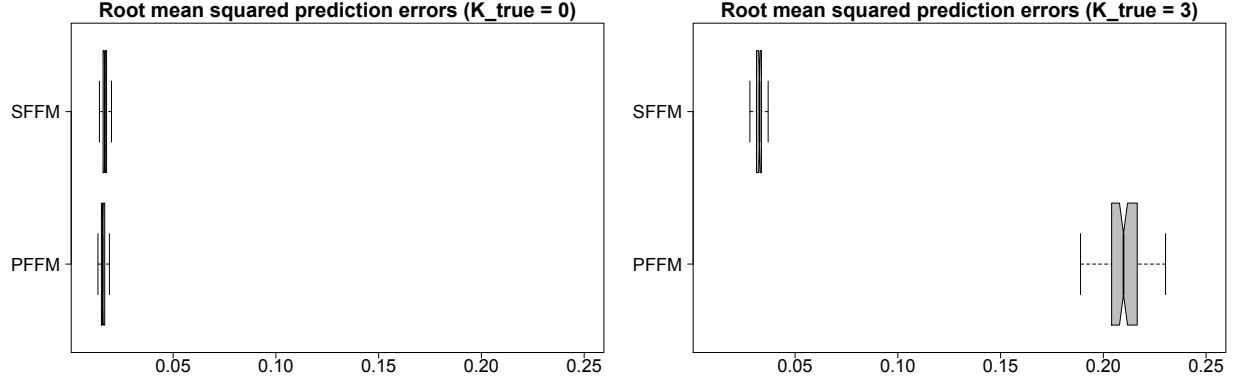


Figure 3: Root mean squared prediction errors for Y^* using the parametric (PFFM) and semi-parametric functional factor models (SFFM) for $K_{true} = 0$ (left) and $K_{true} = 3$ (right). The SFFM maintains point prediction accuracy in both settings, while the PFFM deteriorates substantially for $K_{true} > 0$. Results for $K_{true} = 1$ are similar to those for $K_{true} = 3$ and are omitted.

interval (estimated using sample quantiles from the relevant posterior predictive draws) and $\mathbf{y}_i^* = (y_i^*(\tau_1), \dots, y_i^*(\tau_m))'$ is distributed identically to \mathbf{y}_i . Both the PFFM and the SFFM achieve the nominal 95% coverage, yet the SFFM provides substantially more narrow intervals—and therefore more precise predictive uncertainty quantification—when $K_{true} > 0$.

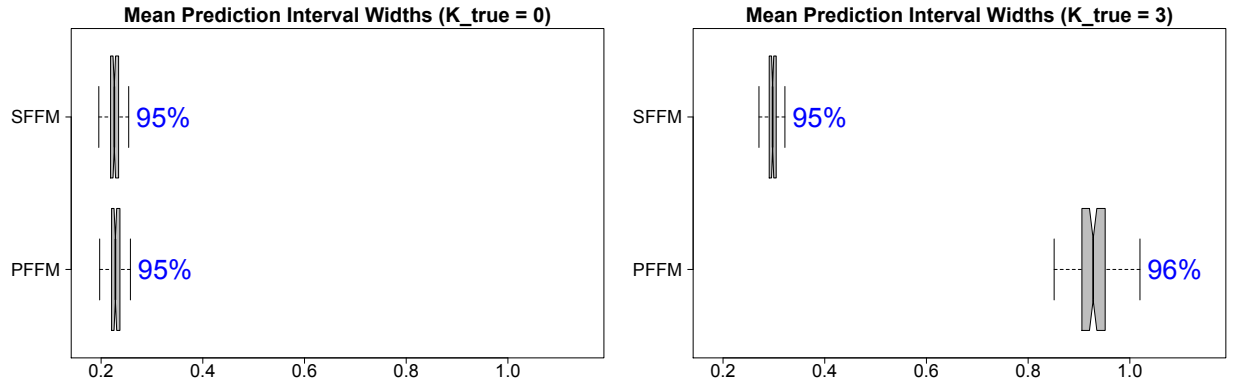


Figure 4: Mean prediction interval widths and empirical coverage for the parametric (PFFM) and semiparametric functional factor models (SFFM) for $K_{true} = 0$ (left) and $K_{true} = 3$ (right). Both models maintain the nominal 95% coverage, but the prediction intervals for SFFM are substantially more narrow—and therefore more precise—when $K_{true} > 0$. Results for $K_{true} = 1$ are similar to those for $K_{true} = 3$ and are omitted.

Inference on the true parametric factors $\{\alpha_{\ell,i}^*\}$ is summarized in Figure 5. Point estimates

(not shown) performed similarly in all cases for the PFFM and SFFM. Posterior credible intervals offer the correct approximate coverage for both the PFFM and the SFFM, yet the PFFM intervals widen substantially when $K_{true} > 0$. This notable result suggests that, even when the goal is inference for the parametric coefficients $\{\alpha_{\ell,i}\}$ —rather than prediction of Y_i —the nonparametric component of the SFFM offers clear benefits.

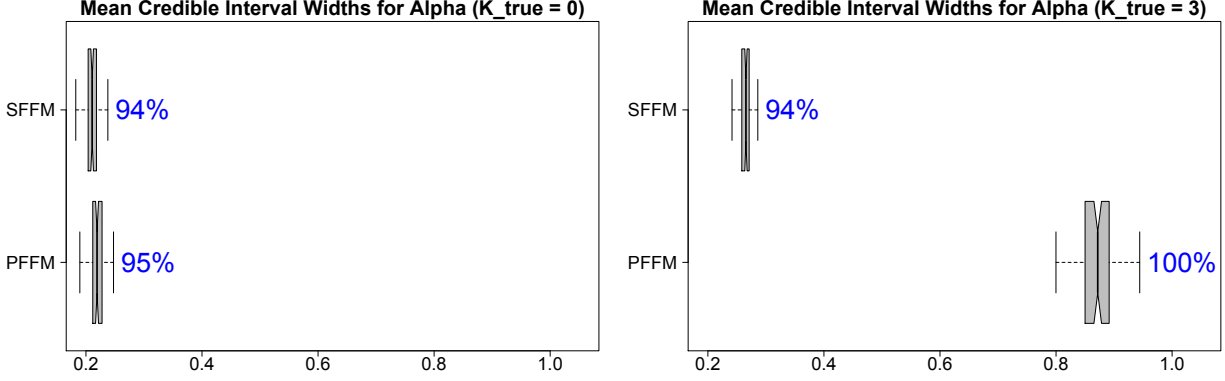


Figure 5: Mean credible intervals widths and empirical coverage for $\{\alpha_{i,\ell}\}$ using the parametric (PFFM) and semiparametric functional factor models (SFFM) for $K_{true} = 0$ (left) and $K_{true} = 3$ (right). Both models maintain approximately the nominal 95% coverage, but the prediction intervals for SFFM are substantially more narrow—and therefore more precise—when $K_{true} > 0$. Results for $K_{true} = 1$ are similar to those for $K_{true} = 3$ and are omitted.

Lastly, we study the posterior distribution of $K^* = \sum_{k=1}^K \mathbb{I}\{z_k > k\}$ for quantifying the necessity of the nonparametric terms. For each simulation, we estimate the posterior probabilities $\mathbb{P}(K^* > 0|\mathbf{y})$ and $\mathbb{P}(|K^* - K_{true}| \leq 1|\mathbf{y})$. Summary statistics for $\mathbb{P}(K^* > 0|\mathbf{y})$ across all simulations are reported in Table 2. When $K_{true} = 0$ and the parametric model is the true data-generating process, the SFFM places little posterior mass on $K^* > 0$ and very rarely places any mass on $K^* > 1$: the minimum value of $\mathbb{P}(|K^* - K_{true}| \leq 1|\mathbf{y}) = \mathbb{P}(K^* \leq 1|\mathbf{y})$ across all simulations is 0.988. When $K_{true} > 0$, the SFFM decisively identifies that $\mathbb{P}(K^* > 0|\mathbf{y}) = 1$ for *all* simulations and is accurate in estimating K^* , with a minimum value of $\mathbb{P}(|K^* - K_{true}| \leq 1|\mathbf{y})$ equal to 0.993 for $K_{true} = 1$ and 0.992 for $K_{true} = 3$.

	Min	1st quartile	Median	3rd quartile	Max
$K_{true} = 0$	0.036	0.058	0.067	0.077	0.114

Table 2: Summary statistics of $\mathbb{P}(K^* > 0|\mathbf{y})$ across 100 simulations when $K_{true} = 0$. When $K_{true} > 0$, we find that $\mathbb{P}(K^* > 0|\mathbf{y}) = 1$ for *all* simulations.

6 Applications

6.1 Pinch force data

Human motor control is a critical area of research with implications for human physiology, monitoring and mitigating muscle degeneration, and designing robotic devices. Motor control data are often recorded at high resolutions and can be modeled as functional data. Important examples include thumb and forefinger pinching (Ramsay et al., 1995), handwriting analysis (Ramsay, 2000), and reaching motions to study the effects of stroke (Goldsmith and Kitago, 2016). In such applications, human physiology and the laws of motion often dictate a parametric model, which is crucial for understanding the underlying process. However, these parametric models may not adequately describe the observed data, which fundamentally undermines the interpretability of the key parameters of interest.

We analyze human pinching data from Ramsay et al. (1995), which reports the force measured by pinching the thumb and forefinger on opposing sides of a 6 cm force meter. The subject was instructed to maintain a background level of constant force, then increase the pinching force to a predetermined maximum level, and finally return to the original background level of constant force. We use data from the `fda` package in R, which consists of $n = 20$ replicate force curves over time each with $m = 151$ observations selected such that the maximum of each curve occurred at 0.076 seconds. An example curve is in Figure 1.

To model the pinch force over time τ , we adapt a parametric model from Ramsay et al. (1995):

$$g_1(\tau; \gamma_i) = 1, \quad g_2(\tau; \gamma_i) = \exp[-(\log \tau - c_i)^2 / \{2 \exp(\gamma_i)\}], \quad (16)$$

where $\exp(c_i)$ is the time of the maximum force and $\gamma_i \in \mathbb{R}$ is a shape parameter. Ramsay et al. (1995) argue that the unnormalized log-normal density g_2 matches the shape of the observed data and offers plausible scientific explanations. For computational convenience, we estimate c_i as in Ramsay et al. (1995) by fitting a quadratic regression in $\log(\tau)$ for the response variable $\log(\mathbf{y}_i)$ restricted to observations $y_i(\tau) > 0.5$. The estimate of each c_i can be recovered from the estimated regression coefficients and is subsequently treated as fixed.

Both PFFMs and SFFMs were fit to the data using the template (16). For partial pooling among subjects, we specify a hierarchical prior on the shape parameters: $\gamma_i \stackrel{iid}{\sim} N(\mu_\gamma, \sigma_\gamma^2)$, $\mu_\gamma \sim N(0, 10)$, and $\sigma_\gamma \sim C^+(0, 1)$, with the priors from (15) on the remaining parameters. Since the nonlinear parameters γ_i are curve-specific, we construct each \mathbf{G}_{γ_i} for $i = 1, \dots, n$ using a QR decomposition as in Section 3.2 and modify the orthogonality constraint to be $\bar{\mathbf{G}}' \mathbf{F} = \mathbf{0}_{L \times K}$ for $\bar{\mathbf{G}} = n^{-1} \sum_{i=1}^n \mathbf{G}_{\gamma_i}$. This constraint no longer preserves the posterior factorization of Corollary 2, but nonetheless maintains the crucial distinctness between the parametric and nonparametric terms. For both models, we retain 10000 MCMC samples after discarding 5000 iterations as a burn-in. Traceplots of $\{Y_i\}$, $\{\alpha_{\ell,i}\}$, and K^* (not shown) demonstrate excellent mixing and suggest convergence.

An example of the fitted values with 95% simultaneous prediction bands for the PFFM and SFFM is in Figure 1. Although the PFFM captures the general shape of the data, it suffers from clear bias around the peak and produces unnecessarily wide prediction bands. The SFFM corrects both issues: the bias is removed and the prediction bands are more precise. Notably, the fitted SFFM curve preserves the same general shape as the PFFM and avoids overfitting despite the increase in modeling complexity.

Posterior uncertainty quantification is also more precise under the SFFM for the parametric factors $\{\alpha_{\ell,i}\}$. Figure 6 presents the posterior standard deviations of $\{\alpha_{\ell,i}\}_{i=1}^n$ for each $\ell = 1, \dots, L$ under the PFFM and SFFM. Although the posterior expectations (not shown) are similar, the posterior standard deviations are substantially smaller under the SFFM. For

model (16), the linear coefficients $\{\alpha_{\ell,i}\}$ determine the maximum of the force curve, which is the most prominent feature in the data. The SFFM provides more precise posterior inference for these key parametric factors.

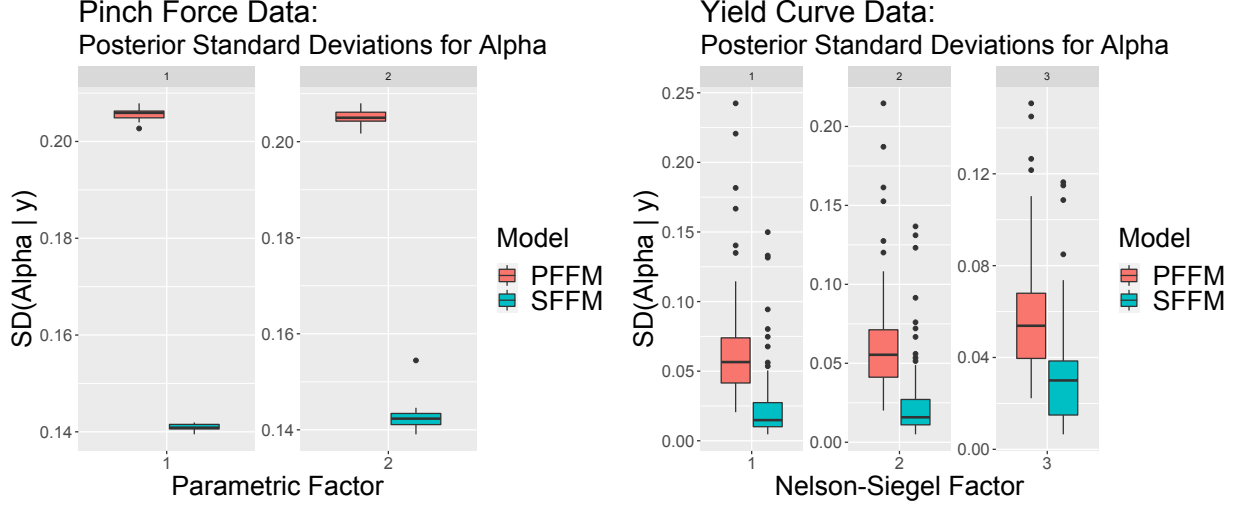


Figure 6: Posterior standard deviations of $\{\alpha_{\ell,i}\}_{i=1}^n$ for $\ell = 1, \dots, L$ in the parametric (PFFM) and semiparametric functional factor model (SFFM) for the pinch force data (left) and yield curve data (right). There is a clear and consistent reduction in posterior uncertainty from the PFFM to the SFFM for these key parametric factors.

Additional evidence in favor of the SFFM is presented in Table 3, which estimates the posterior distribution of the effective number of nonparametric terms K^* . Clearly, there is substantially posterior probability for at least two nonparametric terms, with limited evidence that more than three terms are needed. WAIC similarly favors the SFFM: the estimates are -922 and -3007 for the PFFM and SFFM, respectively.

k	0	1	2	3	4	5	≥ 6
$\mathbb{P}(K^* = k \mathbf{y})$	0.003	0.147	0.707	0.135	0.007	0.001	0

Table 3: Posterior probabilities $\mathbb{P}(K^* = k | \mathbf{y})$ for the pinch force data. There is strong evidence for a nonparametric component.

6.2 Dynamic yield curves

Yield curves play a fundamental role in economic and financial analyses: they provide essential information about current and future economic conditions, including inflation, business cycles, and monetary policies, and are used to price fixed-income securities and construct forward curves. The yield curve $Y_i(\tau)$ describes how interest rates vary as a function of the length of the borrowing period, or time to maturity τ , at each time i . Naturally, yield curves can be modeled as functional data that evolve dynamically over time.

Yield curve models most commonly employ the parametric Nelson-Siegel basis (Nelson and Siegel, 1987):

$$g_1(\tau; \gamma) = 1, \quad g_2(\tau; \gamma) = \{1 - \exp(-\tau\gamma)\}/(\tau\gamma), \quad g_3(\tau; \gamma) = g_2(\tau; \gamma) - \exp(-\tau\gamma) \quad (17)$$

where g_1 is the *level*, g_2 is the *slope*, and g_3 is the *curvature*. The nonlinear parameter $\gamma > 0$ is commonly treated as fixed, such as $\gamma = 0.0609$ (Diebold and Li, 2006; Bianchi et al., 2009), but otherwise may be estimated (Laurini and Hotta, 2010; Cruz-Marcelo et al., 2011). We use a weakly informative Gamma prior for γ with prior mean 0.0609 and prior variance 0.5. Both the PFFM and the SFFM with this prior on γ are favored by WAIC over their respective counterparts with fixed $\gamma = 0.0609$.

To capture the yield curve dynamics, we model the parametric Nelson-Siegel factors as an AR(1):

$$\alpha_{\ell,i} = \mu_\ell + \phi_\ell(\alpha_{\ell,i-1} - \mu_\ell) + \zeta_{\ell,i}, \quad \zeta_{\ell,i} \stackrel{indep}{\sim} N(0, \sigma_{\zeta_\ell}^2). \quad (18)$$

The PFFM with (17) and (18) is also known as the *dynamic Nelson-Siegel model* (Diebold and Li, 2006). The dynamic Nelson-Siegel factors $\{\alpha_{\ell,i}\}$ equivalently may be viewed as the state variables in a dynamic linear model (West and Harrison, 1997). Importantly, the orthogonality constraints on $\{g_\ell\}$ and $\{f_k\}$ admit a convenient and low-dimensional state

space simulation smoothing algorithm for efficient joint sampling of the dynamic factors $\{\alpha_{\ell,i}\}$; see the supplementary material for details.

The dynamic model (18) is accompanied by a diffuse prior $\mu_\ell \stackrel{iid}{\sim} N(0, 10^6)$ and a weakly informative prior $(\phi_\ell + 1)/2 \stackrel{iid}{\sim} \text{Beta}(5, 2)$ —which ensures stationarity of the dynamic factors $\{\alpha_{\ell,i}\}$ and therefore $\{Y_i\}$ and $\{\mathbf{y}_i\}$ —along with $\sigma_{\zeta_\ell} \stackrel{iid}{\sim} C^+(0, 1)$ for $\ell = 1, \dots, L$. In addition, we generalize (2) to accommodate stochastic volatility in the observation error variance:

$$\epsilon_{i,j} \stackrel{indep}{\sim} N(0, \sigma_{\epsilon_i}^2), \quad \log \sigma_{\epsilon_i}^2 \sim \text{AR}(1) \quad (19)$$

which is an essential component in many economic and financial models (Kim et al., 1998). For these AR(1) parameters, we adopt the priors and sampling algorithm from Kowal (2020).

We evaluate the suitability of the Nelson-Siegel basis for modeling monthly unsmoothed Fama and Bliss (1987) US government bond yields from 2000-2009 ($n = 120$) provided by Van Dijk et al. (2014). These data are available for maturities of 3, 6, 9, 12, 15, 18, 21, 24, 30, 36, 48, 60, 72, 84, 96, 108 and 120 months ($m = 17$). Unlike other datasets such as Gürkaynak et al. (2007), these data are *not* pre-smoothed using the Nelson-Siegel basis and therefore provide more robust insights in the efficacy of the Nelson-Siegel template. The inferential targets are the latent curves Y_i , the dynamic Nelson-Siegel factors $\{\alpha_{i,\ell}\}$, and the effective number of nonparametric terms K^* . The MCMC specifications from Section 6.1 are adopted here, again with excellent mixing and convergence for these key parameters.

Figure 1 shows the PFFM and SFFM fitted values with 95% simultaneous prediction bands for the yield curve in September 2008 during the onset of the Great Recession. The PFFM produces a reasonable shape for the yield curve, yet—as with the pinch force data—suffers from clear bias and overconservative prediction bands. The SFFM corrects these deficiencies without distorting the general shape of the curve or overfitting to the data.

Similar results are obtained in Figure 6 for the dynamic Nelson-Siegel factors. The SFFM

offers substantial reductions in posterior standard deviation for all three dynamic Nelson-Siegel factors. These factors are fundamental for describing the shape of the yield curve; reducing the posterior uncertainty is a crucial advantage of the SFFM. Importantly, the simulation study confirms that the reduced posterior uncertainty quantification from the SFFM nonetheless retains valid calibration, or more specifically, correct nominal coverage of the posterior credible intervals.

We summarize the posterior distribution $\mathbb{P}(K^*|\mathbf{y})$ of the effective number of nonparametric terms in Table 4. Notably, the evidence for the nonparametric factors is moderate: we estimate $\mathbb{P}(K^* > 0|\mathbf{y}) = 0.09$. As a reference point, 94% of the synthetic Nelson-Siegel datasets in our simulation study resulted in smaller values of $\mathbb{P}(K^* > 0|\mathbf{y})$ under the null model $K_{true} = 0$, which suggests adequate control of false positives.

k	0	1	2	≥ 3
$\mathbb{P}(K^* = k \mathbf{y})$	0.910	0.087	0.003	0

Table 4: Posterior probabilities $\mathbb{P}(K^* = k|\mathbf{y})$ for the yield curve data. There is moderate evidence for a nonparametric component.

Beyond the evidence in Table 4, there are other compelling reasons to include the nonparametric factors in a dynamic Nelson-Siegel model. First, the uncertainty quantification for $\{Y_i\}$ and $\{\alpha_{\ell,i}\}$ is more precise in the SFFM than in the PFFM (see Figures 1 and 6). Second, WAIC decisively prefers the SFFM (-10229) over the PFFM (-5516), which suggests potential improvements in out-of-sample predictive capabilities. Third, the additional computational burdens of the SFFM are minimal. Due to the orthogonality constraints, the sampling steps for $\{\alpha_{\ell,i}\}$ and associated parameters are identical for the PFFM and the SFFM, which permits full and robust model development for the parametric factors. Further, the computational cost associated with sampling the nonparametric terms is small: the computing time per 1000 iterations is 21s and 23s for the PFFM and SFFM, respectively (using R on a MacBook Pro, 2.8 GHz Intel Core i7).

7 Discussion

We proposed a Bayesian model for semiparametric functional data analysis. The model augments a parametric template with an infinite-dimensional nonparametric functional basis. Crucially, the nonparametric component is regularized with an ordered spike-and-slab prior, which implicitly provides rank selection for infinite-dimensional models and satisfies appealing theoretical properties. This prior is accompanied by a parameter-expansion scheme customized to boost MCMC efficiency, and is broadly applicable for Bayesian (functional, spatial, and temporal) factor models. The nonparametric basis functions are learned from the data but constrained to be orthogonal to the parametric basis functions, which preserves distinctness between the parametric and nonparametric components and offers key computational simplifications. Our analyses of synthetic data, human motor control data, and dynamic interest rates demonstrate clear advantages of the semiparametric modeling framework relative to parametric alternatives. The proposed approach eliminates bias, reduces excessive posterior and predictive uncertainty, and provides reliable inference on the effective number of nonparametric terms—all with minimal additional computational costs.

There are several promising extensions that remain for future work. First, formulation of the parametric template in (1) can be generalized, for example to include a functional regression term with scalar or functional covariates. Second, the ordered spike-and-slab prior currently uses independent and identically distributed variables in the parameter expansion (7). Adaptations to include dependence among these variables, such as regression models, clustering, and spatio-temporal dependence, would broaden the applicability of the prior. Lastly, we studied only a small subset of many possible parametric templates. For applications that rely on such parametric models, the proposed semiparametric modeling framework can directly assess the adequacy of these models—and perhaps suggest improvements.

Acknowledgements

Research was sponsored by the Army Research Office and was accomplished under Grant Number W911NF-20-1-0184. The views and conclusions contained in this document are those of the authors and should not be interpreted as representing the official policies, either expressed or implied, of the Army Research Office or the U.S. Government. The U.S. Government is authorized to reproduce and distribute reprints for Government purposes notwithstanding any copyright notation herein.

References

- Bhattacharya, A. and Dunson, D. B. (2011). Sparse Bayesian infinite factor models. *Biometrika*, 98(2):291–306.
- Bianchi, F., Mumtaz, H., and Surico, P. (2009). The great moderation of the term structure of UK interest rates. *Journal of Monetary Economics*, 56(6):856–871.
- Canale, A., Lijoi, A., Nipoti, B., and Prünster, I. (2017). On the Pitman-Yor process with spike and slab base measure. *Biometrika*, 104(3):681–697.
- Chen, S. T., Xiao, L., and Staicu, A.-M. (2019). Model Testing for Generalized Scalar-on-Function Linear Models.
- Cruz-Marcelo, A., Ensor, K. B., and Rosner, G. L. (2011). Estimating the term structure with a semiparametric Bayesian hierarchical model: An application to corporate bonds. *Journal of the American Statistical Association*, 106(494):387–395.
- Diebold, F. X. and Li, C. (2006). Forecasting the term structure of government bond yields. *Journal of Econometrics*, 130(2):337–364.
- Durante, D. (2017). A note on the multiplicative gamma process. *Statistics and Probability Letters*, 122:198–204.
- Fama, E. F. and Bliss, R. R. (1987). The information in long-maturity forward rates. *The American Economic Review*, pages 680–692.
- Gelman, A. (2006). Prior distributions for variance parameters in hierarchical models. *Bayesian Analysis*, 1(3):515–534.

- Goldsmith, J. and Kitago, T. (2016). Assessing systematic effects of stroke on motor control by using hierarchical function-on-scalar regression. *Journal of the Royal Statistical Society. Series C: Applied Statistics*, 65(2):215–236.
- Goldsmith, J., Zipunnikov, V., and Schrack, J. (2015). Generalized multilevel function-on-scalar regression and principal component analysis. *Biometrics*, 71(2):344–353.
- Gürkaynak, R. S., Sack, B., and Wright, J. H. (2007). The U.S. Treasury yield curve: 1961 to the present. *Journal of Monetary Economics*, 54(8):2291–2304.
- Hays, S., Shen, H., and Huang, J. Z. (2012). Functional dynamic factor models with application to yield curve forecasting. *Annals of Applied Statistics*, 6(3):870–893.
- Heckman, N. E. and Ramsay, J. O. (2000). Penalized regression with model-based penalties. *Canadian Journal of Statistics*, 28(2):241–258.
- Ishwaran, H. and James, L. F. (2001). Gibbs sampling methods for stick-breaking priors. *Journal of the American Statistical Association*, 96(453):161–173.
- Ishwaran, H. and Rao, J. S. (2005). Spike and slab variable selection: Frequentist and Bayesian strategies. *Annals of Statistics*, 33(2):730–773.
- Jauch, M., Hoff, P. D., and Dunson, D. B. (2019). Monte Carlo simulation on the Stiefel manifold via polar expansion. *arXiv preprint arXiv:1906.07684*.
- Kim, S., Shephard, N., and Chib, S. (1998). Stochastic Volatility: Likelihood Inference and Comparison with ARCH Models. *Review of Economic Studies*, 65(3):361–393.
- Kowal, D. R. (2019). Integer-valued functional data analysis for measles forecasting. *Biometrics*, 75(4):1321–1333.
- Kowal, D. R. (2020). Dynamic Regression Models for Time-Ordered Functional Data. *Bayesian Analysis*.
- Kowal, D. R. and Bourgeois, D. C. (2020). Bayesian Function-on-Scalars Regression for High-Dimensional Data. *Journal of Computational and Graphical Statistics*, pages 1–26.
- Kowal, D. R., Matteson, D. S., and Ruppert, D. (2017a). A Bayesian Multivariate Functional Dynamic Linear Model. *Journal of the American Statistical Association*, 112(518):733–744.

- Kowal, D. R., Matteson, D. S., and Ruppert, D. (2017b). Functional autoregression for sparsely sampled data. *Journal of Business & Economic Statistics*, pages 1–13.
- Laurini, M. P. and Hotta, L. K. (2010). Bayesian extensions to Diebold-Li term structure model. *International Review of Financial Analysis*, 19(5):342–350.
- Lee, W., Miranda, M. F., Rausch, P., Baladandayuthapani, V., Fazio, M., Downs, J. C., and Morris, J. S. (2018). Bayesian semiparametric functional mixed models for serially correlated functional data, with application to glaucoma data. *Journal of the American Statistical Association*.
- Legramanti, S., Durante, D., and Dunson, D. B. (2020). Bayesian cumulative shrinkage for infinite factorizations. *Biometrika*, 107(3):745–752.
- Mikulich, S. K., Zerbe, G. O., Jones, R. H., and Crowley, T. J. (2003). Comparing linear and nonlinear mixed model approaches to cosinor analysis. *Statistics in medicine*, 22(20):3195–3211.
- Molenberghs, G. and Verbeke, G. (2000). *Linear mixed models for longitudinal data*. Springer.
- Montagna, S., Tokdar, S. T., Neelon, B., and Dunson, D. B. (2012). Bayesian Latent Factor Regression for Functional and Longitudinal Data. *Biometrics*, 68(4):1064–1073.
- Nelson, C. R. and Siegel, A. F. (1987). Parsimonious Modeling of Yield Curves. *The Journal of Business*, 60(4):473.
- O’Hara, R. B. and Sillanpää, M. J. (2009). A review of Bayesian variable selection methods: What, how and which. *Bayesian Analysis*, 4(1):85–117.
- Ramsay, J. O. (2000). Functional components of variation in handwriting. *Journal of the American Statistical Association*, 95(449):9–15.
- Ramsay, J. O. and Dalzell, C. J. (1991). Some tools for functional data analysis. *Journal of the Royal Statistical Society: Series B (Methodological)*, 53(3):539–561.
- Ramsay, J. O. and Silverman, B. W. (2005). *Functional Data Analysis*. Springer.
- Ramsay, J. O., Wang, X., and Flanagan, R. (1995). A functional data analysis of the pinch force of human fingers. *Journal of the Royal Statistical Society: Series C (Applied Statistics)*, 44(1):17–30.

- Sang, P., Wang, L., and Cao, J. (2017). Parametric functional principal component analysis. *Biometrics*, 73(3):802–810.
- Scarpa, B. and Dunson, D. B. (2009). Bayesian hierarchical functional data analysis via contaminated informative priors. *Biometrics*, 65(3):772–780.
- Scarpa, B. and Dunson, D. B. (2014). Enriched stick-breaking processes for functional data. *Journal of the American Statistical Association*, 109(506):647–660.
- Scheipl, F., Fahrmeir, L., and Kneib, T. (2012). Spike-and-slab priors for function selection in structured additive regression models. *Journal of the American Statistical Association*, 107(500):1518–1532.
- Suarez, A. J. and Ghosal, S. (2017). Bayesian estimation of principal components for functional data. *Bayesian Analysis*, 12(2):311–333.
- Ullah, S. and Finch, C. F. (2013). Applications of functional data analysis: A systematic review. *BMC medical research methodology*, 13(1):43.
- Van Dijk, D., Koopman, S. J., der Wel, M., and Wright, J. H. (2014). Forecasting interest rates with shifting endpoints. *Journal of Applied Econometrics*, 29(5):693–712.
- Wagner, A. B., Hill, E. L., Ryan, S. E., Sun, Z., Deng, G., Bhadane, S., Martinez, V. H., Wu, P., Li, D., Anand, A., Acharya, J., and Matteson, D. S. (2020). Social Distancing Has Merely Stabilized COVID-19 in the US. *Stat*, page e302.
- Wang, Y. (2011). *Smoothing Splines: Methods and Applications*. CRC Press.
- Watanabe, S. (2010). Asymptotic equivalence of Bayes cross validation and widely applicable information criterion in singular learning theory. *Journal of Machine Learning Research*, 11(Dec):3571–3594.
- Welham, S. J., Cullis, B. R., Kenward, M. G., and Thompson, R. (2006). The analysis of longitudinal data using mixed model L-splines. *Biometrics*, 62(2):392–401.
- West, M. and Harrison, J. (1997). *Bayesian Forecasting and Dynamic Models*. Springer.
- Wood, S. (2006). *Generalized additive models: an introduction with R*. CRC press.